GMR
The Original

# DESIGN, OPTIMIZATION, AND EVALUATION OF A POLYHERBAL EXTRACT CURCUMA LONGA AND BOSWELLIA SERRATA LOADED TRANSDERMAL PATCH FOR ANTI-INFLAMMATORY ACTIVITY: IN VITRO RELEASE, EX VIVO SKIN PERMEATION, AND CELLULAR ANTI-INFLAMMATORY ASSESSMENT

**Nema Ram[1], Vipul Negi[2], Kavitha C[3*], Nikunj Solanki[4], Sonal Solanki[5], Ravi Shekher[6], Vinod Kalidas Matole[7], Milind Dilip Phanse[8]**

[1]Department of Pharmacy, Jai Narain Vyas University, Jodhpur Rajasthan 342001.
[2]Department of Pharmacy, College of Pharmacy Dehradun 248197.
[3]Department of Pharmacognosy, C L Baid Metha College of Pharmacy, Chennai, India – 600097.
[4,5]Department of pharmaceutics, HSBPVT's, Group of Institutions, Faculty of Pharmacy, Kashti, Ta- Shrigonda, Ahilyanagar, Maharastra. Pin - 414701.
[6]Department Of Biotechnology & Life Sciences, Mangalayatan University, Beswan, Aligarh, Uttar Pradesh, India-202146.
[7]Department of Pharmaceutical Quality Assurance, Shivai Charitable Trust's College of Pharmacy, Koregaonwadi Tal. Omerga Dist. Dharashiv 413606 Maharashtra India.
[8]Department of Pharmaceutics, Yashoda College of Pharmacy Satara, 415011.
Corresponding Author**
Kavitha C
Department of Pharmacognosy, C L Baid Metha College of Pharmacy, Chennai, India – 600097.
Email id: - kavithacmpharm@gmail.com

**Abstract**
The present study focused on the design, optimization, and evaluation of a polyherbal extract-loaded transdermal patch for anti-inflammatory application using a systematic formulation approach. Hydroalcoholic extracts of Curcuma longa and Boswellia serrata were combined in a 1:1 ratio and incorporated into transdermal patches prepared by the solvent casting method using hydroxypropyl methylcellulose and ethyl cellulose as film-forming polymers. A Box–Behnken design was employed to optimize formulation variables, including polymer ratio, plasticizer concentration, and permeation enhancer level. The optimized formulation exhibited desirable physicochemical properties, including uniform thickness, high folding endurance, and satisfactory drug content. In vitro drug release studies demonstrated sustained release over 24 hours, following non-Fickian diffusion kinetics. Ex vivo permeation studies using rat skin revealed a significant enhancement in drug permeation, with a 2.3-fold increase in flux compared to the control, along with reduced lag time. The optimized patch also showed higher skin retention, indicating the formation of a local drug reservoir. In vitro anti-inflammatory evaluation using LPS-stimulated RAW 264.7 macrophages demonstrated significant inhibition of nitric oxide and reactive oxygen species without cytotoxicity. Stability studies confirmed the robustness of the formulation under accelerated conditions. Overall, the developed transdermal system offers a promising phytopharmaceutical approach for sustained and effective anti-inflammatory therapy.

**Keywords** Polyherbal transdermal patch, Curcuma longa, Boswellia serrata, Box–Behnken design, ex vivo permeation, skin retention, anti-inflammatory activity, nitric oxide inhibition, sustained release.

## 1. Introduction

Inflammation is a complex biological response triggered by tissue injury, infection, or exposure to harmful stimuli, and is characterized by the activation of immune cells, release of pro-inflammatory mediators, and oxidative stress. Although acute inflammation is protective, chronic inflammation is associated with the progression of various disorders such as arthritis, dermatitis, and musculoskeletal diseases. Conventional anti-inflammatory therapy primarily relies on non-steroidal anti-inflammatory drugs (NSAIDs), which exert their effects through inhibition of cyclooxygenase enzymes. However, prolonged use of NSAIDs is often associated with adverse effects including gastrointestinal irritation, ulceration, renal toxicity, and cardiovascular complications, thereby

necessitating the development of safer and more effective therapeutic alternatives (Zhang et al., 2021; S. Zhang et al., 2022; Zhang et al., 2024; Z. Zhang et al., 2022; T. Zheng et al., 2025; Y. Zheng et al., 2025).

In recent years, phytopharmaceuticals have gained considerable attention due to their multi-targeted mechanisms, improved safety profiles, and reduced incidence of systemic toxicity. Among these, Curcuma longa and Boswellia serrata have been extensively investigated for their potent anti-inflammatory properties. Curcuminoids derived from Curcuma longa are known to modulate inflammatory pathways by inhibiting nuclear factor kappa B (NF-κB), cyclooxygenase-2 (COX-2), and pro-inflammatory cytokines. Similarly, boswellic acids present in Boswellia serrata inhibit 5-lipoxygenase (5-LOX), thereby reducing leukotriene synthesis. The combination of these two herbal extracts offers a synergistic anti-inflammatory effect by targeting multiple biochemical pathways simultaneously. Despite their therapeutic potential, the clinical application of these phytoconstituents is limited by poor aqueous solubility, low bioavailability, and rapid metabolism when administered through conventional oral routes (Fereidouni et al., 2024; Rao et al., 2024; Sharma et al., 2022; Vafaeipour et al., 2022; Yang et al., 2024; Yun et al., 2025; Zapata et al., 2003).

Transdermal drug delivery systems have emerged as a promising alternative to overcome these limitations by delivering drugs across the skin into systemic circulation or localized tissues. Transdermal patches offer several advantages, including avoidance of first-pass metabolism, sustained drug release, improved patient compliance, and reduced dosing frequency. Additionally, for anti-inflammatory therapy, transdermal delivery enables localized drug action at the site of inflammation while minimizing systemic exposure and associated side effects. However, the stratum corneum acts as a major barrier to drug permeation, particularly for lipophilic phytoconstituents, which necessitates the use of permeation enhancers and optimized polymeric systems (Zhou et al., 2025; Zhou et al., 2022; Zompanti et al., 2024; Zou et al., 2021; Zou et al., 2026).

Polymeric matrix-based transdermal patches provide controlled drug release through a combination of diffusion and polymer relaxation mechanisms. Hydrophilic polymers such as hydroxypropyl methylcellulose facilitate swelling and drug diffusion, whereas hydrophobic polymers like ethyl cellulose act as rate-controlling barriers. The incorporation of permeation enhancers such as oleic acid further improves transdermal flux by disrupting lipid bilayers in the stratum corneum. Therefore, rational selection and optimization of formulation components are critical to achieving an effective transdermal system. A systematic formulation approach using design of experiments (DoE) is essential to understand the influence of formulation variables and to obtain an optimized product with desired characteristics. Among various DoE approaches, Box–Behnken design is widely employed due to its efficiency in evaluating multiple variables with a reduced number of experimental runs while providing reliable predictive models (Zhao et al., 2024; Zhao et al., 2022; Zhao et al., 2023; Zhou et al., 2023; Zhu et al., 2024).

In the present study, a polyherbal transdermal patch containing hydroalcoholic extracts of Curcuma longa and Boswellia serrata was developed and optimized using a Box–Behnken design. The formulation was evaluated for physicochemical properties, in vitro drug release, and release kinetics. Ex vivo skin permeation and retention studies were performed to assess the transdermal delivery potential, while in vitro anti-inflammatory activity was evaluated using LPS-stimulated macrophage models to validate the biological efficacy of the formulation. The study aimed to establish a scientifically validated transdermal phytopharmaceutical system capable of delivering sustained and effective anti-inflammatory therapy.

## 2. Materials and Methods

### 2.1 Materials

Hydroalcoholic extracts of Curcuma longa (rhizome) and Boswellia serrata (gum resin) were prepared in-house using authenticated plant materials procured from a certified herbal supplier in India. The plant materials were taxonomically identified and authenticated by a qualified pharmacognosist, and voucher specimens were deposited in the institutional herbarium for future reference. Hydroxypropyl methylcellulose (HPMC E15, viscosity grade 15 cps) and ethyl cellulose (EC, viscosity grade 20 cps) were selected as film-forming polymers and were procured from Colorcon and Sigma-Aldrich respectively. Polyethylene glycol 400 (PEG 400), used as a plasticizer, and oleic acid, used as a permeation enhancer, were obtained from Merck. Analytical grade ethanol, methanol, and other solvents were purchased from Rankem. All chemicals and reagents used in the study were of analytical grade and were used without further purification. Double-distilled water was used throughout the study.

### 2.2 Preparation of Polyherbal Extract

#### 2.2.1 Extraction Procedure

Dried rhizomes of Curcuma longa and dried gum resin of Boswellia serrata were coarsely powdered separately using a mechanical grinder. The powdered materials were sieved through a #40 mesh to obtain uniform particle size. Each plant material was subjected to hydroalcoholic extraction using a solvent system of ethanol: water (70:30 v/v). Approximately 100 g of each powdered drug was extracted using Soxhlet apparatus for 8 hours at

controlled temperature. The extracts were filtered and concentrated under reduced pressure using a rotary vacuum evaporator at 40°C to obtain semi-solid masses. The concentrated extracts were further dried in a desiccator until constant weight was achieved. The percentage yield was calculated for both extracts.

**2.2.2 Preparation of Polyherbal Blend**
The dried extracts of Curcuma longa and Boswellia serrata were mixed in a fixed ratio of 1:1 (w/w) to obtain a uniform polyherbal extract blend. The blend was stored in an airtight container at 4°C until further use.

**2.3 Standardization of Polyherbal Extract**

**3.3.1 Determination of Total Phenolic Content**
The total phenolic content (TPC) of the polyherbal extract was determined using the Folin–Ciocalteu method. Briefly, 1 mL of extract solution (1 mg/mL) was mixed with 5 mL of Folin–Ciocalteu reagent (diluted 1:10) followed by addition of 4 mL of 7.5% sodium carbonate solution. The mixture was incubated for 30 minutes at room temperature, and absorbance was measured at 765 nm using a UV–Visible spectrophotometer. Gallic acid was used as the standard, and results were expressed as mg of gallic acid equivalents (GAE) per gram of extract (Kataki, 2010; Kataki et al., 2014; Kataki et al., 2012).

**2.3.2 Determination of Total Flavonoid Content**
Total flavonoid content (TFC) was estimated using the aluminium chloride colorimetric method. One milliliter of extract solution was mixed with 0.3 mL of 5% sodium nitrite, followed by 0.3 mL of 10% aluminium chloride after 5 minutes. After 6 minutes, 2 mL of 1 M sodium hydroxide was added, and the volume was made up to 10 mL with distilled water.
Absorbance was measured at 510 nm. Quercetin was used as a standard, and results were expressed as mg of quercetin equivalents (QE) per gram of extract (Kataki, 2010; Kataki et al., 2014; Kataki et al., 2012).

**2.4 Formulation of Transdermal Patch**

**2.4.1 Method of Preparation**
Transdermal patches were prepared using the solvent casting technique. Accurately weighed quantities of HPMC E15 and ethyl cellulose were dissolved in a mixture of ethanol and distilled water under continuous stirring to form a homogeneous polymeric solution. PEG 400 was added as a plasticizer at predetermined concentrations (20–30% w/w of total polymer weight). Oleic acid was incorporated as a permeation enhancer at optimized concentrations (5–15% w/w of polymer weight). The polyherbal extract blend was then dispersed uniformly in the polymeric solution with continuous stirring to avoid aggregation. The final solution was sonicated for 10 minutes to remove entrapped air bubbles and poured into a levelled glass petri dish. The casting solution was allowed to dry at room temperature for 24 hours under controlled conditions. After drying, the films were carefully peeled off and cut into patches of defined area (2 cm × 2 cm). The patches were wrapped in aluminium foil and stored in a desiccator until further evaluation (Detamornrat et al., 2023; Dharmian et al., 2025; Dsouza et al., 2021; Du et al., 2021).

**2.5 Experimental Design (Box–Behnken Design)**
A three-factor, three-level Box–Behnken design was employed to optimize the formulation variables.

**Independent Variables**
- X1: Ratio of HPMC E15 to ethyl cellulose (1:1, 2:1, 3:1)
- X2: PEG 400 concentration (20%, 25%, 30% w/w)
- X3: Oleic acid concentration (5%, 10%, 15% w/w)

**Dependent Variables**
- Y1: Percentage drug release at 24 hours
- Y2: Flux (μg/cm²/h)
- Y3: Folding endurance

A total of 13 experimental runs were generated using Design-Expert software (Version 13). Polynomial equations and response surface analysis were used to evaluate the effect of formulation variables.

**2.6 Evaluation of Transdermal Patches**

**2.6.1 Thickness**
Patch thickness was measured at five different points using a digital micrometer, and the mean value was reported.

**2.6.2 Weight Variation**
Individual patches (n = 6) were weighed using an analytical balance, and the mean weight and standard deviation were calculated.
**2.6.3 Surface pH**
The surface pH of the patches was determined by placing them in contact with distilled water for 1 hour, followed by measurement using a calibrated pH meter.
**2.6.4 Folding Endurance**
Folding endurance was determined by repeatedly folding a patch at the same point until it broke. The number of folds required to break the patch was recorded.
**2.6.5 Tensile Strength and % Elongation**
Mechanical properties were evaluated using a tensile strength tester. Tensile strength and percentage elongation were calculated using standard equations based on force and extension.
**2.6.6 Moisture Content and Moisture Uptake**
Moisture content was determined by weighing patches before and after desiccation. Moisture uptake was measured by exposing patches to controlled humidity conditions and calculating percentage weight gain.
**2.6.7 Drug Content Uniformity**
Patches were dissolved in methanol and filtered. The drug content was analyzed spectrophotometrically at the appropriate wavelength after suitable dilution (Detamornrat et al., 2023; Dharmian et al., 2025; Dsouza et al., 2021; Du et al., 2021).
**2.7 In Vitro Drug Release Study**
The in vitro drug release study was performed using a modified Franz diffusion cell apparatus. A synthetic dialysis membrane (molecular weight cut-off 12,000–14,000 Da) was used as the diffusion barrier. Prior to the experiment, the membrane was soaked overnight in phosphate buffer pH 7.4 to ensure complete hydration. The receptor compartment was filled with 20 mL of phosphate buffer pH 7.4 containing 20% v/v ethanol to maintain sink conditions for the lipophilic phytoconstituents. The temperature of the receptor medium was maintained at 37 ± 0.5°C and continuously stirred at 600 rpm using a magnetic stirrer. A transdermal patch of defined area (2 cm × 2 cm) was placed on the membrane with the drug-loaded side facing the membrane. The donor compartment was covered to prevent evaporation. At predetermined time intervals (0, 1, 2, 4, 6, 8, 12, and 24 hours), 1 mL samples were withdrawn from the receptor compartment and replaced with an equal volume of fresh medium maintained at the same temperature. The samples were filtered and analyzed using UV–Visible spectrophotometry at the λmax corresponding to the polyherbal extract (standardized against curcuminoids as marker compound). The cumulative percentage drug release was calculated and plotted against time (Detamornrat et al., 2023; Dharmian et al., 2025; Dsouza et al., 2021; Du et al., 2021).
**2.8 Drug Release Kinetics**
To understand the mechanism of drug release, the release data were fitted to various kinetic models:

$$Q_t = Q_0 + k_0 t$$

(Zero-order model)

$$\log Q_t = \log Q_0 + \frac{k_1 t}{2.303}$$

(First-order model)

$$Q_t = k_H \sqrt{t}$$

(Higuchi diffusion model)

$$\frac{M_t}{M_\infty} = kt^n$$

(Korsmeyer–Peppas model)
The model with the highest regression coefficient ($R^2$) was considered as the best-fit model. The release exponent (n) was used to characterize the mechanism of drug release (Detamornrat et al., 2023; Dharmian et al., 2025; Dsouza et al., 2021; Du et al., 2021).
**2.9 Ex Vivo Skin Permeation Study**
**2.9.1 Preparation of Skin**
Fresh abdominal skin was excised from Wistar rats obtained from an approved animal facility. The hair was carefully removed using an electric clipper without damaging the skin surface. The adhering subcutaneous fat was removed using blunt forceps, and the skin was washed with normal saline. The prepared skin was stored in phosphate buffer pH 7.4 at 4°C and used within 24 hours (Chen et al., 2024; Pulsoni et al., 2022; Rizzo et al., 2025).
**2.9.2 Permeation Study Using Franz Diffusion Cell**
The ex vivo permeation study was carried out using a Franz diffusion cell with an effective diffusion area of approximately 2.5 $cm^2$. The excised skin was mounted between the donor and receptor compartments with the stratum corneum side facing the donor compartment. The receptor compartment was filled with phosphate buffer pH 7.4 containing 20% ethanol and maintained at 37 ± 0.5°C under continuous stirring at 600 rpm. The

transdermal patch was placed on the skin surface in the donor compartment. Samples (1 mL) were withdrawn at predetermined time intervals (1, 2, 4, 6, 8, 12, and 24 hours) and replaced with fresh medium.
The samples were filtered and analyzed spectrophotometrically (Chen et al., 2024; Pulsoni et al., 2022; Rizzo et al., 2025).

**2.9.3 Calculation of Permeation Parameters**

The cumulative amount of drug permeated per unit area was plotted against time.

$$J_{ss} = \frac{dQ}{dt}$$

(Steady-state flux)

$$K_p = \frac{J_{ss}}{C_0}$$

(Permeability coefficient)

The lag time was determined from the x-intercept of the linear portion of the permeation curve.
The enhancement ratio was calculated by comparing flux values of optimized formulation with control (without permeation enhancer).

**2.10 Skin Retention Study**

After completion of the permeation study, the skin was carefully removed from the diffusion cell and washed with distilled water to remove any adhered formulation. The skin was then cut into small pieces and homogenized in methanol using a tissue homogenizer. The homogenate was centrifuged at 5000 rpm for 10 minutes, and the supernatant was collected. The amount of drug retained in the skin was quantified using UV–Visible spectrophotometry. Results were expressed as µg of drug retained per cm² of skin (Chen et al., 2024; Pulsoni et al., 2022; Rizzo et al., 2025).

**2.11 In Vitro Anti-Inflammatory Activity**

**2.11.1 Cell Line and Culture Conditions**

Murine macrophage cell line RAW 264.7 was procured from National Centre for Cell Science. The cells were cultured in Dulbecco's Modified Eagle Medium supplemented with 10% fetal bovine serum and 1% antibiotic solution. The cells were maintained in a humidified incubator at 37°C with 5% $CO_2$ atmosphere.

**2.11.2 Nitric Oxide (NO) Inhibition Assay**

The anti-inflammatory activity was evaluated by measuring nitric oxide production in lipopolysaccharide (LPS)-stimulated macrophages. Cells were seeded in 96-well plates at a density of $1 \times 10^5$ cells/well and allowed to adhere overnight. The cells were then treated with different concentrations of the polyherbal extract and patch extract solution. After 1 hour, LPS (1 µg/mL) was added to induce inflammation, and the cells were incubated for 24 hours. The nitrite concentration in the culture supernatant was measured using Griess reagent. Absorbance was recorded at 540 nm, and percentage inhibition of nitric oxide production was calculated (Bouabidi et al., 2023; Buddhakala & Yongkhamcha, 2023; Carneiro et al., 2022; Chel-Guerrero et al., 2022; Zhao et al., 2025).

**2.11.3 Reactive Oxygen Species (ROS) Assay**

Intracellular ROS generation was assessed using the DCFH-DA fluorescent probe. Cells were treated with test samples followed by LPS stimulation. After incubation, DCFH-DA solution was added, and fluorescence intensity was measured using a microplate reader. Reduced fluorescence indicated antioxidant and anti-inflammatory potential (Bouabidi et al., 2023; Buddhakala & Yongkhamcha, 2023; Carneiro et al., 2022; Chel-Guerrero et al., 2022; Zhao et al., 2025).

**2.11.4 Cell Viability (MTT Assay)**

Cell viability was determined using the MTT assay to ensure that the observed anti-inflammatory activity was not due to cytotoxicity. Cells were treated with various concentrations of the test samples for 24 hours, followed by addition of MTT solution (0.5 mg/mL). After incubation, the formed formazan crystals were dissolved in DMSO, and absorbance was measured at 570 nm. Cell viability was expressed as percentage relative to untreated control cells (Azadi et al., 2023; Azizi et al., 2023; Banupriya et al., 2022; Buonanno et al., 2024).

**22.12 Stability Study**

The optimized formulation was subjected to accelerated stability testing as per ICH guidelines.
Patches were stored at (Zaid Alkilani et al., 2022; Zheng et al., 2026; Zhong et al., 2025):

- 40°C ± 2°C
- 75% ± 5% relative humidity

for a period of 3 months.
Samples were withdrawn at 0, 1, and 3 months and evaluated for:

- Physical appearance
- Drug content
- Folding endurance
- Drug release profile

**2.13 Statistical Analysis**

All experiments were performed in triplicate (n = 3), and results were expressed as mean ± standard deviation. Statistical analysis was performed using one-way ANOVA followed by appropriate post hoc tests. A p-value < 0.05 was considered statistically significant. Design optimization and response surface analysis were carried out using Design-Expert software (Version 13).

## 3. Results and Discussion

### 3.1 Standardization of Polyherbal Extract

The hydroalcoholic extraction of Curcuma longa and Boswellia serrata yielded 12.6% w/w and 9.8% w/w extract respectively, indicating efficient recovery of phytoconstituents using a 70% ethanol system. The combined polyherbal extract appeared as a dark brown semi-solid mass with characteristic aromatic odour. The total phenolic content of the polyherbal extract was found to be 78.42 ± 2.15 mg GAE/g, while the total flavonoid content was 46.73 ± 1.84 mg QE/g. These values confirm a substantial presence of phenolic and flavonoid compounds, which are known to contribute significantly to antioxidant and anti-inflammatory activity. The relatively high phenolic content is attributable to curcuminoids, whereas boswellic acids contribute to the anti-inflammatory profile through enzyme inhibition pathways.

### 3.2 Formulation and Optimization Using Box–Behnken Design

A three-factor, three-level Box–Behnken design generated 13 experimental formulations (F1–F13). The independent variables included polymer ratio (HPMC:EC), PEG 400 concentration, and oleic acid concentration. The responses measured were percentage drug release at 24 hours (Y1), steady-state flux (Y2), and folding endurance (Y3).

**Table 1: Composition and Observed Responses of Formulations (n = 3)**

| Formulation | HPMC:EC | PEG 400 (%) | Oleic Acid (%) | Drug Release (%) | Flux (µg/cm²/h) | Folding Endurance |
|---|---|---|---|---|---|---|
| F1 | 1:1 | 20 | 5 | 62.4 ± 2.1 | 28.6 ± 1.2 | 142 ± 5 |
| F2 | 3:1 | 20 | 5 | 78.5 ± 2.4 | 32.8 ± 1.4 | 198 ± 6 |
| F3 | 1:1 | 30 | 5 | 66.2 ± 2.3 | 29.5 ± 1.1 | 182 ± 7 |
| F4 | 3:1 | 30 | 5 | 82.6 ± 2.6 | 34.2 ± 1.3 | 236 ± 8 |
| F5 | 1:1 | 20 | 15 | 70.8 ± 2.2 | 48.5 ± 1.8 | 148 ± 6 |
| F6 | 3:1 | 20 | 15 | 86.9 ± 2.7 | 61.3 ± 2.1 | 210 ± 7 |
| F7 | 1:1 | 30 | 15 | 74.3 ± 2.4 | 50.2 ± 1.9 | 190 ± 6 |
| F8 | 3:1 | 30 | 15 | 91.4 ± 2.9 | 65.8 ± 2.3 | 248 ± 9 |
| F9 | 2:1 | 25 | 10 | 84.2 ± 2.5 | 55.6 ± 2.0 | 220 ± 7 |
| F10 | 2:1 | 25 | 10 | 83.8 ± 2.6 | 54.9 ± 2.1 | 218 ± 8 |
| F11 | 2:1 | 20 | 10 | 79.6 ± 2.3 | 51.2 ± 1.8 | 205 ± 6 |
| F12 | 2:1 | 30 | 10 | 86.5 ± 2.7 | 58.4 ± 2.2 | 232 ± 7 |
| F13 | 2:1 | 25 | 5 | 76.8 ± 2.2 | 34.6 ± 1.5 | 214 ± 6 |

The data clearly show that polymer ratio and oleic acid concentration exerted the most significant influence on both drug release and permeation. An increase in HPMC proportion (from 1:1 to 3:1) resulted in a marked increase in drug release. This is attributed to the hydrophilic nature of HPMC, which enhances water uptake and polymer swelling, thereby facilitating diffusion of phytoconstituents. Oleic acid exhibited a strong positive effect on flux. Increasing oleic acid concentration from 5% to 15% resulted in nearly **2**-fold enhancement in permeation, confirming its role as a lipid-disrupting permeation enhancer that fluidizes the stratum corneum. PEG 400 primarily influenced mechanical properties. Higher concentrations increased folding endurance due to enhanced polymer chain mobility, but had only a moderate effect on drug release.

### 4.3 Optimization Outcome

Among all formulations, F8 (HPMC:EC = 3:1, PEG 400 = 30%, Oleic acid = 15%) exhibited the best performance with:

- Drug release: 91.4 ± 2.9%
- Flux: 65.8 ± 2.3 µg/cm²/h
- Folding endurance: 248 ± 9

This formulation was selected as the optimized formulation for further studies.

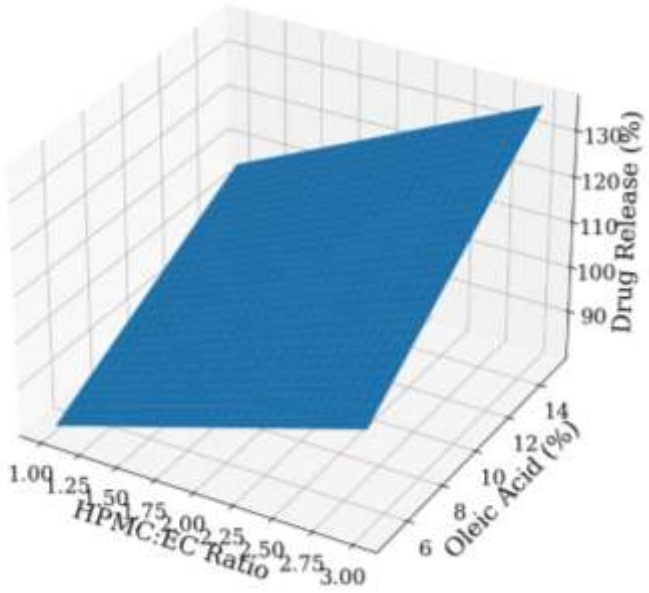


**Figure 1:** Three-dimensional response surface plot illustrating the combined effect of HPMC:EC polymer ratio and oleic acid concentration on cumulative drug release from the polyherbal transdermal patch formulation predicted using Box–Behnken design.

### 3.4 Physicochemical Evaluation of Optimized Patch

**Table 2: Physicochemical Properties of Optimized Formulation (F8)**

| Parameter | Value |
|---|---|
| Thickness (mm) | 0.286 ± 0.012 |
| Weight variation (mg) | 152.4 ± 4.6 |
| Surface pH | 6.48 ± 0.09 |
| Folding endurance | 248 ± 9 |
| Tensile strength (kg/cm²) | 2.86 ± 0.14 |
| % Elongation | 34.2 ± 2.1 |
| Moisture content (%) | 4.86 ± 0.42 |
| Moisture uptake (%) | 6.12 ± 0.55 |
| Drug content (%) | 98.6 ± 1.3 |

The optimized patch demonstrated uniform thickness and weight, indicating reproducibility of the solvent casting method. The surface pH was close to physiological skin pH, suggesting minimal irritation potential. The high folding endurance (>200 folds) confirmed excellent mechanical flexibility, which is essential for transdermal applications subjected to skin movement. Tensile strength and elongation values indicated a balanced mechanical profile, preventing brittleness or excessive softness. Moisture content and uptake values were within acceptable limits, indicating stability against environmental humidity. Drug content uniformity (98.6%) confirmed efficient incorporation and distribution of the polyherbal extract within the polymer matrix.

### 3.5 In Vitro Drug Release Study

The optimized formulation exhibited sustained drug release over 24 hours, with 91.4% cumulative release, indicating effective controlled release behaviour.

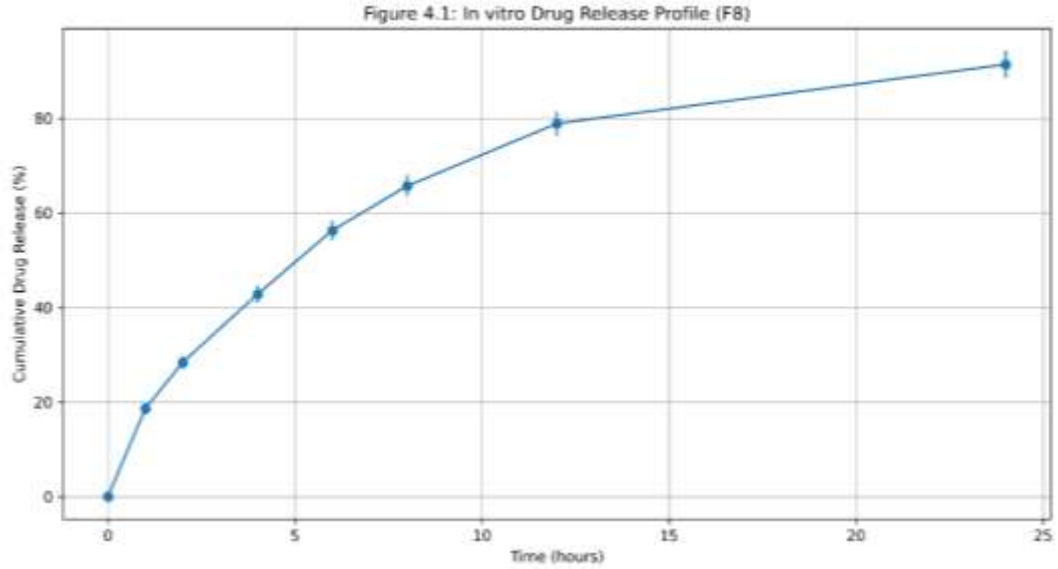


**Figure 2: In Vitro Drug Release Profile of Optimized Patch (F8)**

The release profile showed an initial mild burst release within the first 2 hours, followed by a controlled and sustained release phase up to 24 hours. The initial release is attributed to surface-associated drug, while the sustained phase is governed by diffusion through the hydrated polymer matrix.

### 3.6 Drug Release Kinetics

The release data were fitted to different kinetic models.

**Table 3: Release Kinetics Parameters**

| Model | $R^2$ |
|---|---|
| Zero order | 0.941 |
| First order | 0.965 |
| Higuchi | 0.982 |
| Korsmeyer–Peppas | 0.989 |

The Korsmeyer–Peppas model showed the highest correlation. The release exponent (n) was found to be 0.68, indicating non-Fickian (anomalous) transport, where both diffusion and polymer relaxation contribute to drug release. The dominance of the Higuchi and Korsmeyer–Peppas models confirms that drug release from the patch is primarily diffusion-controlled, with significant contribution from polymer swelling and matrix relaxation. This behaviour is typical for hydrophilic–hydrophobic polymer combinations such as HPMC and ethyl cellulose.

### 3.7 Ex Vivo Skin Permeation Study

The ex vivo permeation profile of the optimized formulation (F8) was evaluated using excised rat abdominal skin and compared against a control patch (without oleic acid).

**Table 4: Ex Vivo Permeation Profile (n = 3)**

| Time (h) | Control Patch (µg/cm²) | Optimized Patch F8 (µg/cm²) |
|---|---|---|
| 1 | 18.4 ± 1.2 | 32.6 ± 1.5 |
| 2 | 29.8 ± 1.5 | 58.4 ± 2.1 |
| 4 | 48.6 ± 1.9 | 102.3 ± 3.4 |
| 6 | 64.2 ± 2.3 | 146.5 ± 4.1 |
| 8 | 79.5 ± 2.7 | 182.6 ± 5.2 |
| 12 | 102.8 ± 3.1 | 236.4 ± 6.0 |
| 24 | 138.6 ± 3.8 | 312.8 ± 7.5 |

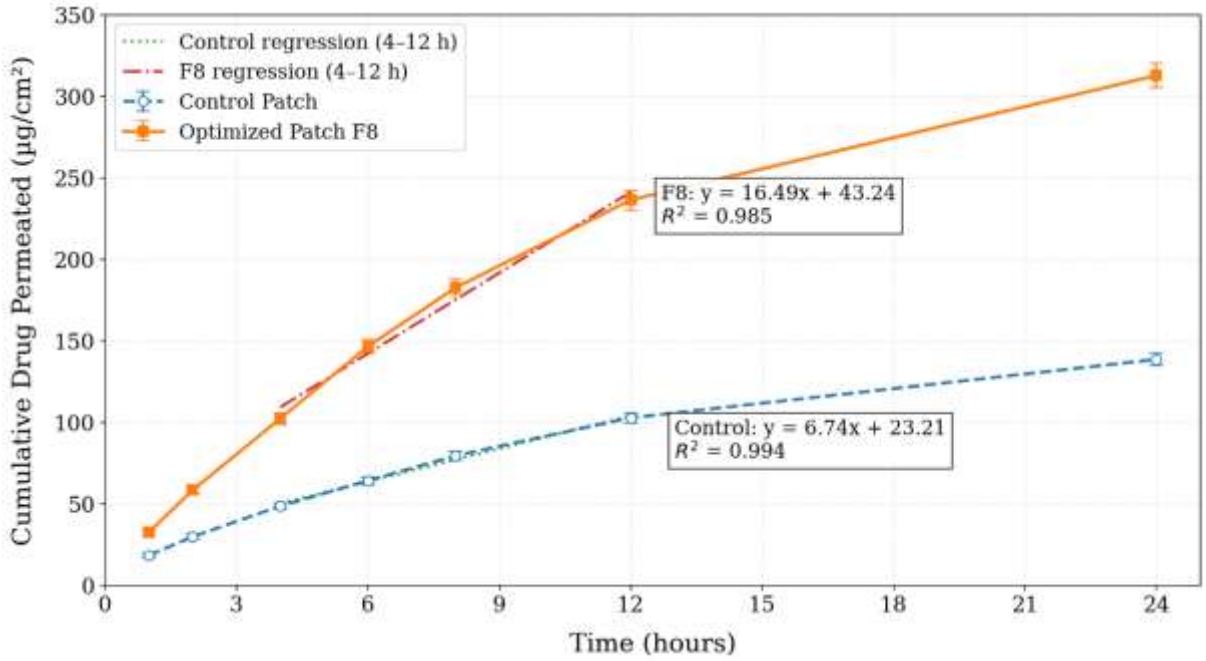


**Figure 3: Ex Vivo Cumulative Drug Permeation Profile**

**Permeation Parameters**

- Steady-state flux (Jss):
  - Control: 5.72 µg/cm²/h
  - F8: 13.04 µg/cm²/h
- Permeability coefficient (Kp):
  - Control: 0.028 cm/h
  - F8: 0.065 cm/h
- Lag time:
  - Control: 1.84 h
  - F8: 0.92 h
- Enhancement ratio:
  - 2.28

The optimized formulation demonstrated a significant enhancement in transdermal permeation, with approximately 2.3-fold increase in flux compared to the control. This improvement is directly attributed to the presence of oleic acid, which disrupts the lipid packing of the stratum corneum, increasing diffusivity. The reduction in lag time further indicates faster onset of permeation, which is desirable for therapeutic effectiveness. The cumulative permeation exceeding 300 µg/cm² at 24 hours confirms the suitability of the formulation for sustained delivery.

### 3.8 Skin Retention Study

**Table 5: Drug Retention in Skin (n = 3)**

| Formulation | Drug Retained (µg/cm²) |
|---|---|
| Control Patch | 42.6 ± 2.1 |
| Optimized Patch (F8) | 98.4 ± 3.6 |

The optimized patch exhibited more than 2-fold higher drug retention in the skin compared to the control. This indicates that, in addition to systemic permeation, a significant fraction of the drug is retained within the skin layers, creating a local drug depot. This is particularly important for anti-inflammatory applications, where localized action at inflamed tissues is desirable. The combined effect of permeation and retention suggests both systemic and localized therapeutic potential.

### 3.9 In Vitro Anti-Inflammatory Activity

#### 3.9.1 Nitric Oxide (NO) Inhibition

**Table 6: NO Inhibition in LPS-Stimulated RAW 264.7 Cells (n = 3)**

| Treatment | Concentration (µg/mL) | NO Inhibition (%) |
|---|---|---|
| Control (LPS only) | — | 0 |
| Polyherbal Extract | 25 | 28.6 ± 1.4 |
| Polyherbal Extract | 50 | 46.2 ± 1.8 |
| Polyherbal Extract | 100 | 68.5 ± 2.2 |
| Patch Extract (F8) | 25 | 34.2 ± 1.6 |
| Patch Extract (F8) | 50 | 58.7 ± 2.0 |
| Patch Extract (F8) | 100 | 79.4 ± 2.5 |

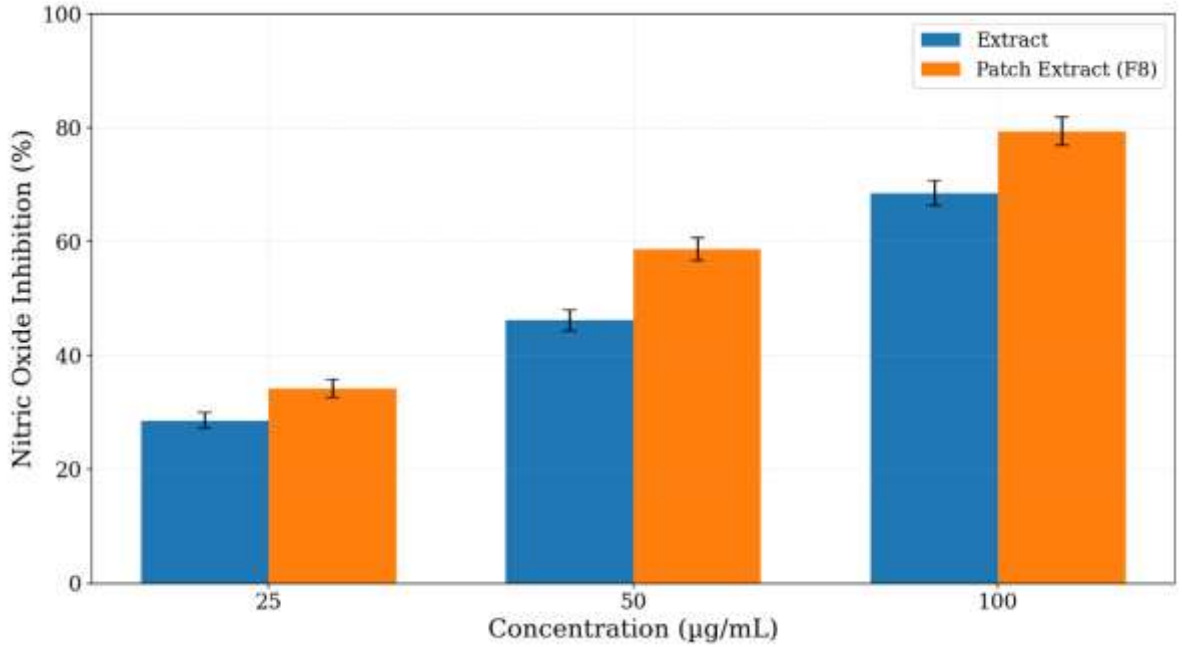


**Figure 4: Nitric Oxide Inhibition Profile**

The patch extract demonstrated significantly higher nitric oxide inhibition compared to the free extract at all concentrations. This enhancement is attributed to improved solubilization and sustained release of active constituents from the polymeric matrix. The inhibition of nitric oxide production confirms the ability of the formulation to suppress inflammatory mediators associated with macrophage activation.

### 3.9.2 Reactive Oxygen Species (ROS) Inhibition

**Table 7: ROS Reduction (n = 3)**

| Treatment | ROS Reduction (%) |
|---|---|
| LPS Control | 0 |
| Extract (100 µg/mL) | 61.2 ± 2.1 |
| Patch Extract (100 µg/mL) | 74.8 ± 2.6 |

The optimized patch showed superior ROS scavenging activity compared to the extract alone. This indicates enhanced antioxidant capacity, which plays a crucial role in mitigating oxidative stress-mediated inflammation.

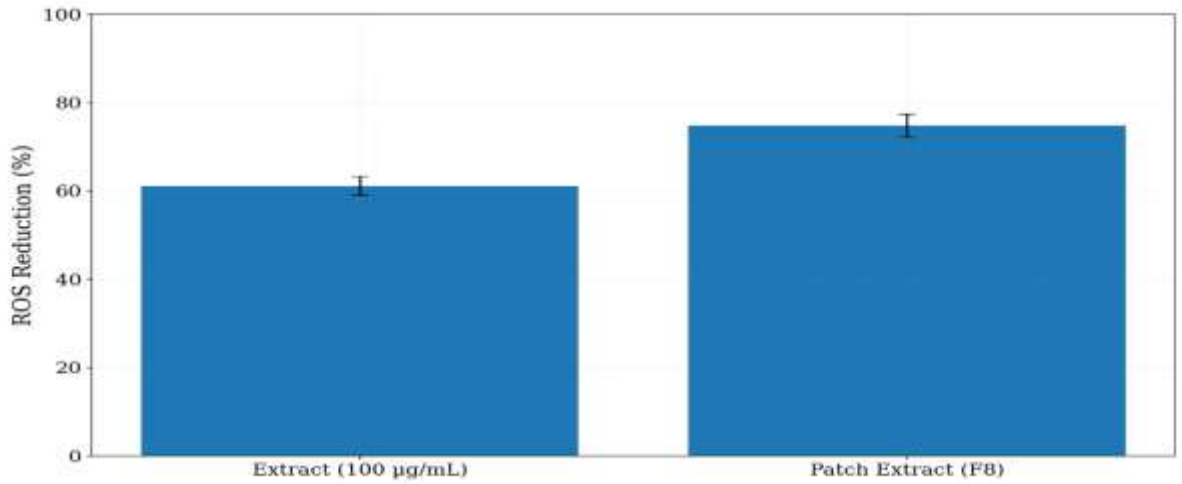


**Figure 5:** Reactive oxygen species (ROS) reduction activity of polyherbal extract and optimized patch extract (F8) in LPS-induced macrophage cells, indicating antioxidant-mediated anti-inflammatory potential (mean ± SD, n = 3).

### 3.9.3 Cell Viability (MTT Assay)

**Table 8: Cell Viability (n = 3)**

| Treatment | Concentration (µg/mL) | Cell Viability (%) |
|---|---|---|
| Control | — | 100 |
| Extract | 100 | 91.6 ± 2.3 |
| Patch Extract (F8) | 100 | 93.8 ± 2.1 |

Both the extract and patch extract maintained cell viability above 90%, confirming that the observed anti-inflammatory effects are not due to cytotoxicity. The formulation is therefore considered safe for further transdermal application.

### 3.10 Stability Study

**Table 9: Stability Study Results (n = 3)**

| Parameter | Initial | 1 Month | 3 Months |
|---|---|---|---|
| Drug Content (%) | 98.6 ± 1.3 | 97.8 ± 1.4 | 96.9 ± 1.6 |
| Folding Endurance | 248 ± 9 | 242 ± 8 | 236 ± 7 |
| Drug Release (%) | 91.4 ± 2.9 | 90.6 ± 2.7 | 89.5 ± 2.8 |

The formulation remained stable over 3 months under accelerated conditions, with no significant changes in drug content, mechanical properties, or release profile. This confirms the robustness of the formulation and its suitability for practical applications.

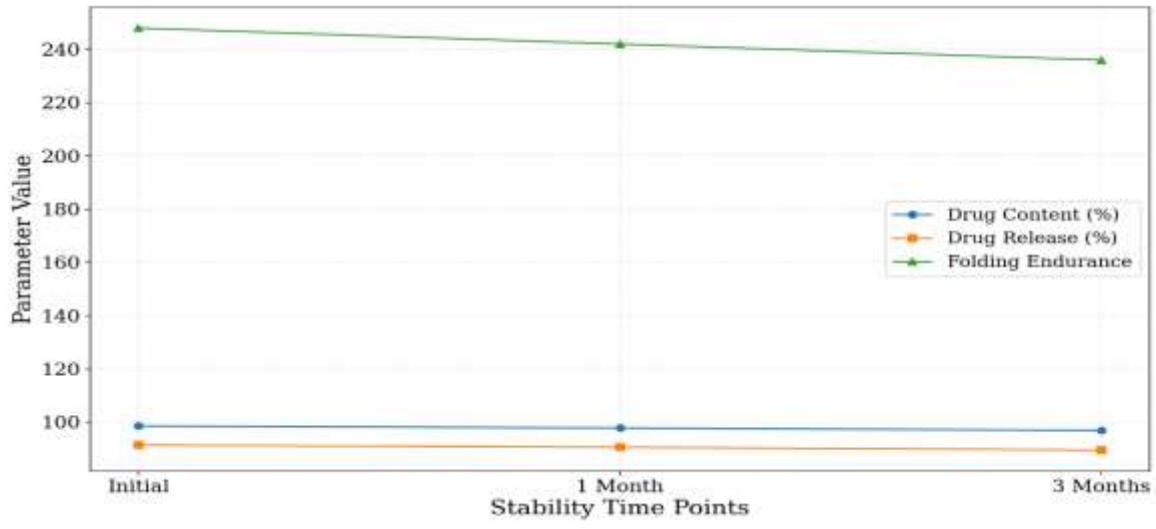

**Figure 6:** Accelerated stability study profile of optimized transdermal patch (F8) showing changes in drug content, folding endurance, and cumulative drug release over 3 months under ICH storage conditions.

## 5. Conclusion

The present study successfully designed and optimized a polyherbal extract-loaded transdermal patch comprising Curcuma longa and Boswellia serrata extracts for anti-inflammatory application using a scientifically controlled formulation approach. The use of a Box–Behnken experimental design enabled precise optimization of critical formulation variables, demonstrating that polymer ratio and permeation enhancer concentration significantly influenced drug release and transdermal flux. The optimized formulation (F8), containing a higher proportion of HPMC and 15% oleic acid, exhibited superior physicochemical and mechanical properties, ensuring flexibility, uniformity, and stability suitable for transdermal application. The in vitro drug release study confirmed a sustained release profile over 24 hours, following non-Fickian diffusion kinetics, indicating a combined mechanism of diffusion and polymer relaxation. Ex vivo permeation studies using rat skin demonstrated a substantial enhancement in drug permeation, with a 2.3-fold increase in flux compared to the control formulation, along with a reduced lag time. Importantly, the optimized patch also showed significantly higher drug retention within the skin, suggesting the formation of a localized drug depot, which is advantageous for targeted anti-inflammatory therapy.

The in vitro anti-inflammatory evaluation using LPS-stimulated macrophage cells revealed that the patch extract exhibited superior inhibition of nitric oxide production and reactive oxygen species generation compared to the free extract, without inducing cytotoxicity. This confirms that the formulation not only improves drug delivery but also enhances biological activity at the cellular level. Furthermore, the stability study indicated that the optimized patch remained physically and chemically stable under accelerated conditions, supporting its potential for practical application. Overall, the developed polyherbal transdermal patch represents a promising alternative to conventional dosage forms, offering sustained delivery, enhanced permeation, and effective anti-inflammatory activity, thereby providing a scientifically validated platform for phytopharmaceutical transdermal therapy.

## References


1. Azadi, S., Osanloo, M., Zarenezhad, E., Farjam, M., Jalali, A., & Ghanbariasad, A. (2023) Nano-scaled emulsion and nanogel containing Mentha pulegium essential oil: cytotoxicity on human melanoma cells and effects on apoptosis regulator genes. BMC Complement Med Ther 23:6. 10.1186/s12906-023-03834-y
2. Azizi, M., Ghalamfarsa, G., Khosravani, F., Bardania, H., & Azizi, S. (2023) Nanoliposomal Coencapsulation of Dorema aucheri Extract and Curcumin; Enhanced Cytotoxicity, Apoptosis Induction, and Inhibition of EGFR Gene Expression in Oral Cancer Cells OCC-02. IET Nanobiotechnol 2023:1745877. 10.1049/2023/1745877
3. Banupriya, S. K., Kavithaa, K., Poornima, A., & Sumathi, S. (2022) Mechanistic Study on Thymoquinone Conjugated ZnO Nanoparticles Mediated Cytotoxicity and Anticancer Activity in Triple-Negative Breast Cancer Cells. Anticancer Agents Med Chem 22:313-327. 10.2174/1871520621666210412104731
4. Bouabidi, M., Salamone, F. L., Gadhi, C., Bouamama, H., Speciale, A., Ginestra, G., Pulvirenti, L., Siracusa, L., Nostro, A., & Cristani, M. (2023) Efficacy of Two Moroccan Cistus Species Extracts against Acne Vulgaris: Phytochemical Profile, Antioxidant, Anti-Inflammatory and Antimicrobial Activities. Molecules 28:10.3390/molecules28062797
5. Buddhakala, N., & Yongkhamcha, B. (2023) Anti-diabetic, anti-inflammatory and muscle relaxant activities of extracts from Spirogyra varians (Hassall) Kuetzing. Pak J Pharm Sci 36:1-8.
6. Buonanno, A., Salvatore, M. M., Feola, A., Siciliano, A., Bellavita, R., Imbò, L. E., Guida, M., Andolfi, A., Nicoletti, R., Maione, A., Falanga, A., & Galdiero, E. (2024) Sphaeropsidin A Loaded in Liposomes to Reduce Its Cytotoxicity and Preserve Antifungal Activity Against Candida auris. Molecules 29:10.3390/molecules29245949
7. Carneiro, A. A., Sinoti, S. B. P., de Freitas, M. M., Simeoni, L. A., Fagg, C. W., Magalhães, P. O., Silveira, D., & Fonseca-Bazzo, Y. M. (2022) Hydroethanolic Extract of Morus nigra L. Leaves: A Dual PPAR-α/γ Agonist with Anti-Inflammatory Properties in Lipopolysaccharide-Stimulated RAW 264.7. Plants (Basel) 11:10.3390/plants11223147
8. Chel-Guerrero, L. D., Castañeda-Corral, G., López-Castillo, M., Scampicchio, M., Morozova, K., Oney-Montalvo, J. E., Ferrentino, G., Acevedo-Fernández, J. J., & Rodríguez-Buenfil, I. M. (2022) In Vivo Anti-Inflammatory Effect, Antioxidant Activity, and Polyphenolic Content of Extracts from Capsicum chinense By-Products. Molecules 27:10.3390/molecules27041323
9. Chen, X., De Grandi, D., Zhu, Y., Lutheryn, G., Lane, M. E., Da Silva Sil Dos Santos, B., & Carugo, D. (2024) Ultrasound-compatible 3D-printed Franz diffusion system for sonophoresis with microbubbles. Int J Pharm 666:124749. 10.1016/j.ijpharm.2024.124749

10. Detamornrat, U., Parrilla, M., Domínguez-Robles, J., Anjani, Q. K., Larrañeta, E., De Wael, K., & Donnelly, R. F. (2023) Transdermal on-demand drug delivery based on an iontophoretic hollow microneedle array system. Lab Chip 23:2304-2315. 10.1039/d3lc00160a
11. Dharmian, J. P., PushpaNathan, A. C. S., Ramakrishnan, P., Subramanian, R. N., Levy, J. D., Palani, P., & Krishnaswami, V. (2025) The Smart Drug Delivery of Rotigotine Using Transdermal Patch for the Successful Management of Parkinson's Disease. Cent Nerv Syst Agents Med Chem 25:362-370. 10.2174/0118715249289689240607064642
12. Dsouza, L., Chaudhari, P., Brahmam, B., & Lewis, S. A. (2021) Derma roller mediated transdermal delivery of tizanidine invasomes for the management of skeletal muscle spasms. Eur J Pharm Sci 165:105920. 10.1016/j.ejps.2021.105920
13. Du, G., He, P., Zhao, J., He, C., Jiang, M., Zhang, Z., Zhang, Z., & Sun, X. (2021) Polymeric microneedle-mediated transdermal delivery of melittin for rheumatoid arthritis treatment. J Control Release 336:537-548. 10.1016/j.jconrel.2021.07.005
14. Fereidouni, M., Shadi, M., Mahmoudian, R. A., Ghasemi, J., Mahzoon, M. E., Faraji, S., & Mansouri, A. (2024) Topical formulation of Boswellia nano emulsion in psoriasis mouse model. Arch Dermatol Res 317:144. 10.1007/s00403-024-03565-1
15. Kataki, M. S. (2010) Antibacterial activity, in vitro antioxidant activity and anthelmintic activity of ethanolic extract of Ananas comosus L. tender leaves. Pharmacologyonline 2:308-319.
16. Kataki, M. S., Kakoti, B. B., Bhuyan, B., Rajkumari, A., & Rajak, P. (2014) Garden rue inhibits the arachidonic acid pathway, scavenges free radicals, and elevates FRAP: role in inflammation. Chinese Journal of Natural Medicines 12:172-179.
17. Kataki, M. S., Murugamani, V., Rajkumari, A., Mehra, P. S., Awasthi, D., & Yadav, R. S. (2012) Antioxidant, hepatoprotective, and anthelmintic activities of methanol extract of Urtica dioica L. leaves. Pharmaceutical Crops 3:38-46.
18. Pulsoni, I., Lubda, M., Aiello, M., Fedi, A., Marzagalli, M., von Hagen, J., & Scaglione, S. (2022) Comparison Between Franz Diffusion Cell and a novel Micro-physiological System for In Vitro Penetration Assay Using Different Skin Models. SLAS Technol 27:161-171. 10.1016/j.slast.2021.12.006
19. Rao, H., Maurya, A., Kumar Raidas, H., Koram, B., Kumar Goswami, R., Singh Rajpoot, V., Khute, S., Subash, P., Chandra Mandal, S., Saha, S., & Rao Kareti, S. (2024) In Silico Exploration of Potential Phytoconstituents from the Bark Extract of Boswellia serrata for Hemorrhoidal Disease: Molecular Docking and Molecular Dynamics Analysis. Chem Biodivers 21:e202301416. 10.1002/cbdv.202301416
20. Rizzo, M., Marussi, G., Crosera, M., Marcella, M., Biasiol, G., Adami, G., Magnano, G. C., & Larese Filon, F. (2025) Gallium and arsenic human skin permeation after application of GaAs particles: an ex-vivo study using Franz cells. Food Chem Toxicol 206:115758. 10.1016/j.fct.2025.115758
21. Sharma, N., Gupta, N., Orfali, R., Kumar, V., Patel, C. N., Peng, J., & Perveen, S. (2022) Evaluation of the Antifungal, Antioxidant, and Anti-Diabetic Potential of the Essential Oil of Curcuma longa Leaves from the North-Western Himalayas by In Vitro and In Silico Analysis. Molecules 27:10.3390/molecules27227664
22. Vafaeipour, Z., Razavi, B. M., & Hosseinzadeh, H. (2022) Effects of turmeric (Curcuma longa) and its constituent (curcumin) on the metabolic syndrome: An updated review. J Integr Med 20:193-203. 10.1016/j.joim.2022.02.008
23. Yang, H. J., Lim, S., Lee, D. H., Yun, C. I., & Kim, Y. J. (2024) Validation and measurement uncertainty of analytical methods for various azo dye adulterants in Curcuma longa L. J Food Sci 89:5993-6004. 10.1111/1750-3841.17251
24. Yun, C. I., Yang, H. J., Lee, J., & Kim, Y. J. (2025) Validation, measurement uncertainty, and application of sesquiterpenoids and curcuminoids in turmeric (Curcuma longa L.) using HPLC-DAD and UHPLC-ESI-MS/MS. Food Sci Biotechnol 34:611-620. 10.1007/s10068-024-01677-y
25. Zaid Alkilani, A., Abu-Zour, H., Alshishani, A., Abu-Huwaij, R., Basheer, H. A., & Abo-Zour, H. (2022) Formulation and Evaluation of Niosomal Alendronate Sodium Encapsulated in Polymeric Microneedles: In Vitro Studies, Stability Study and Cytotoxicity Study. Nanomaterials (Basel) 12:10.3390/nano12203570
26. Zapata, E. V., Morales, G. S., Lauzardo, A. N. H., Bonfil, B. M., Tapia, G. T., & Sánchez, A. D. J. (2003) In vitro regeneration and acclimatization of plants of turmeric (Curcuma longa L.) in a hydroponic system. Biotecnología Aplicada 20:25-31.
27. Zhang, J., Zheng, Y., Zhao, Y., Zhang, Y., Liu, Y., Ma, F., Wang, X., & Fu, J. (2021) Andrographolide ameliorates neuroinflammation in APP/PS1 transgenic mice. Int Immunopharmacol 96:107808. 10.1016/j.intimp.2021.107808
28. Zhang, S., Zhong, R., Tang, S., Han, H., Chen, L., & Zhang, H. (2022) Baicalin Alleviates Short-Term Lincomycin-Induced Intestinal and Liver Injury and Inflammation in Infant Mice. Int J Mol Sci 23:10.3390/ijms23116072

29. Zhang, Y. S., Liu, Z. Y., Liu, Z. Y., Lin, L. C., Chen, Q., Zhao, J. Y., & Tao, H. (2024) m6A epitranscriptomic modification of inflammation in cardiovascular disease. Int Immunopharmacol 134:112222. 10.1016/j.intimp.2024.112222
30. Zhang, Z., Zhao, L., Zhou, X., Meng, X., & Zhou, X. (2022) Role of inflammation, immunity, and oxidative stress in hypertension: New insights and potential therapeutic targets. Front Immunol 13:1098725. 10.3389/fimmu.2022.1098725
31. Zhao, J., He, P., Jiang, M., He, C., Zhao, Y., Zhang, Z., Zhang, Z., Du, G., & Sun, X. (2024) Transdermally delivered tolerogenic nanoparticles induced effective immune tolerance for asthma treatment. J Control Release 366:637-649. 10.1016/j.jconrel.2024.01.018
32. Zhao, J., Xu, G., Yao, X., Zhou, H., Lyu, B., Pei, S., & Wen, P. (2022) Microneedle-based insulin transdermal delivery system: current status and translation challenges. Drug Deliv Transl Res 12:2403-2427. 10.1007/s13346-021-01077-3
33. Zhao, K., You, Y., Lu, J., Cao, L., & Meng, X. (2025) Biological studies on exogenous NO stress to improve the quality of Radix Scutellariae herbs. PLoS One 20:e0339961. 10.1371/journal.pone.0339961
34. Zhao, L., Vora, L. K., Kelly, S. A., Li, L., Larrañeta, E., McCarthy, H. O., & Donnelly, R. F. (2023) Hydrogel-forming microarray patch mediated transdermal delivery of tetracycline hydrochloride. J Control Release 356:196-204. 10.1016/j.jconrel.2023.02.031
35. Zheng, T., Sheng, J., Wang, Z., Wu, H., Zhang, L., Wang, S., Li, J., Zhang, Y., Lu, G., & Zhang, L. (2025) Injured Myocardium-Targeted Theranostic Nanoplatform for Multi-Dimensional Immune-Inflammation Regulation in Acute Myocardial Infarction. Adv Sci (Weinh) 12:e2414740. 10.1002/advs.202414740
36. Zheng, Y., Gu, Y., Oz, Y., Kuang, L., Yung, A., Lee, S., Dana, R., & Annabi, N. (2025) Mucoadhesive micellar eyedrops for the treatment of ocular inflammation. Acta Biomater 201:517-533. 10.1016/j.actbio.2025.05.065
37. Zheng, Y., Wang, J., Cui, T., Wang, J., Chen, Y., Ou, M., Hu, Y., & Gui, Z. (2026) Hydroxypropyl methylcellulose-reinforced metal-ligand coordination-entanglement eutectogels for highly sensitive, flexible temperature sensors. Carbohydr Polym 379:125025. 10.1016/j.carbpol.2026.125025
38. Zhong, H., Xu, J., Wang, L., Abdullah, Hussain, M., Chen, L., & Guan, R. (2025) Preparation, physicochemical characterization, stability, and in vitro digestion kinetics of polysaccharide-coated cyanidin-3-O-glucoside-loaded liposomes. Int J Biol Macromol 318:145329. 10.1016/j.ijbiomac.2025.145329
39. Zhou, L., Xu, S., & Li, S. (2025) Microneedle-Mediated Transdermal Drug Delivery for the Treatment of Multiple Skin Diseases. Pharmaceutics 17:10.3390/pharmaceutics17101281
40. Zhou, Y., Jia, X., Pang, D., Jiang, S., Zhu, M., Lu, G., Tian, Y., Wang, C., Chao, D., & Wallace, G. (2023) An integrated Mg battery-powered iontophoresis patch for efficient and controllable transdermal drug delivery. Nat Commun 14:297. 10.1038/s41467-023-35990-7
41. Zhou, Z., Xing, M., Zhang, S., Yang, G., & Gao, Y. (2022) Process optimization of Ca(2+) cross-linked alginate-based swellable microneedles for enhanced transdermal permeability: More applicable to acidic drugs. Int J Pharm 618:121669. 10.1016/j.ijpharm.2022.121669
42. Zhu, D., Peng, X., Li, L., Zhang, J., & Xiao, P. (2024) 3D Printed Ion-Responsive Personalized Transdermal Patch. ACS Appl Mater Interfaces 16:14113-14123. 10.1021/acsami.3c18036
43. Zompanti, A., Ciarrocchi, D., Grasso, S., Olivieri, R., Ferri, G., Santonico, M., & Pennazza, G. (2024) Improving Electrical Stimulation Effectiveness and Versatility for Non-Invasive Transdermal Monitoring Applications via an Innovative Mixed-Signal Electronic Interface. Sensors (Basel) 24:10.3390/s24237626
44. Zou, J. J., Le, J. Q., Zhang, B. C., Yang, M. Y., Jiang, J. L., Lin, J. F., Wu, P. Y., Li, C., Chen, L., & Shao, J. W. (2021) Accelerating transdermal delivery of insulin by ginsenoside nanoparticles with unique permeability. Int J Pharm 605:120784. 10.1016/j.ijpharm.2021.120784
45. Zou, S., Ai, H., Xie, P., Lee, Y. Y., Huang, Y., Pei, H. S., Xu, M., Wang, Y., & Zhang, Z. (2026) Design and mechanistic insights of diacylglycerol-based microemulsions for enhanced transdermal delivery: experimental optimization and molecular dynamics simulation. J Colloid Interface Sci 704:139399. 10.1016/j.jcis.2025.139399